LAWRENCE
LIVERMORE
NATIONAL
LABORATORY

Selective Thermal Reduction of Single-layer MoO3 nanostructures on Au(111)

X. Deng, S.Y. Quek, M.M. Biener, J. Biener, D.H. Kang, R. Schalek, E. Kaxiras, C.M. Firend

December 11, 2007

Surface Science

Disclaimer

This document was prepared as an account of work sponsored by an agency of the United States government. Neither the United States government nor Lawrence Livermore National Security, LLC, nor any of their employees makes any warranty, expressed or implied, or assumes any legal liability or responsibility for the accuracy, completeness, or usefulness of any information, apparatus, product, or process disclosed, or represents that its use would not infringe privately owned rights. Reference herein to any specific commercial product, process, or service by trade name, trademark, manufacturer, or otherwise does not necessarily constitute or imply its endorsement, recommendation, or favoring by the United States government or Lawrence Livermore National Security, LLC. The views and opinions of authors expressed herein do not necessarily state or reflect those of the United States government or Lawrence Livermore National Security, LLC, and shall not be used for advertising or product endorsement purposes.

Selective Thermal Reduction of Single-layer MoO$_3$ nanostructures on Au(111)

[1]Xingyi Deng, [2]Su Ying Quek, [1, 2, 5]Monika M. Biener, [3, 5]Juergen Biener, [1]Dae Hyuk Kang,
[3]Richard Schalek, [2, 4]Efthimios Kaxiras, [1, 2]Cynthia M. Friend*

[1]Department of Chemistry and Chemical Biology, [2]Division of Engineering and Applied
Sciences, [3]Center for Nanoscale Science, and [4]Department of Physics
Harvard University, Cambridge, MA 02138, USA
[5]Nanoscale Synthesis and Characterization Laboratory, Lawrence Livermore National
Laboratory, Livermore, California 94550, USA

Abstract

MoO$_3$ is an interesting oxide prototype because its catalytic activity is sensitive to the
presence and nature of defects. In this work, we demonstrate that we can control the number of
defects in single-layer MoO$_3$ nanostructures grown on Au(111) by a simple thermal reduction
treatment. X-ray photoelectron spectroscopy demonstrates the formation of Mo^{5+} species and
oxygen vacancies during annealing at 650 K. The percentage of Mo^{5+} increases with the duration
of annealing, until a stable composition containing 50% Mo^{6+} and 50% Mo^{5+} is obtained.
Surprisingly, the formation of lower oxidation states such as Mo^{4+} was not observed. The
reduced MoO$_x$ islands remain one layer high, based on scanning tunneling microscope (STM)
images. The two-dimensional nature of the reduced oxide nanocrystals may be due to a large
barrier for structural reorganization and, thus, may account for the absence of Mo oxidation
states lower than +5. Based on scanning tunneling microscopy images and density functional
calculations, we propose that the formation of Mo^{5+} ions during annealing is not associated with
formation of oxygen point defects, but can be attributed to the formation of extended one-
dimensional shear defects. These reduced structures are useful for studying the dependence of
reactivity on defect type, and present exciting possibilities for chemical sensors and other
applications.

_____

Selective Thermal Reduction of Single-layer MoO$_3$…, Deng, etal. SUSC-D—06-00862

1

microscopy, Defects, Molybdenum oxides, Density functional calculations, Nanostructures, Au(111), Catalysis

Selective Thermal Reduction of Single-layer MoO$_3$…, Deng, etal. SUSC-D—06-00862

2

Introduction

Metal oxides constitute an important class of commercial catalysts [2]. For example, supported MoO_3 promotes the partial oxidation of methane to formaldehyde and is widely used as a catalyst in the petroleum and chemical industry [3-6]. The catalytic properties of metal oxides depend sensitively on the presence and nature of defects. In the case of molybdenum oxides, a high surface oxidation state is expected to be a crucial factor for partial oxidation of hydrocarbons [7]; on the other hand, the presence of oxygen vacancies plays an important role in enhancing selectivity and reactivity by providing reactive sites [8]. Thus the ability to control quantity and type of defects present in the oxides is important, both for fundamental studies and for applications.

In recent years, novel metal oxide nanocrystals have been grown on metal surfaces[9] [Quek, 2005 #3805;Biener, 2004 #3533]. This development adds another dimension of interest because these nanocrystals often exhibit structures and electronic properties that are distinct from the bulk phase, and which arise from interface [Altieri, 2001 #4007;Sinnott, 2003 #4008] and nanoscale [10-12] effects. The ability to grow such structures in a controllable fashion thus opens the door for many novel applications. Previously, we demonstrated that *crystalline* two-dimensional MoO_3 nanostructures on Au(111) can be synthesized on Au(111) via oxidation of Mo nanoclusters using NO_2 as oxidizing reagent [13], [14]. Whilst bulk MoO_3 is a bilayered material, these MoO_3 nanocrystals exhibit a unique single-layer structure with Au replacing the other half of the bilayer. Epitaxy with the Au(111) substrate is achieved via straining the in-plane Mo-O bonds which gives rise to electronic properties that are different from bulk MoO_3 [1]. The well-defined and novel structure of these nanocrystals provides an interesting starting point for the synthesis of reduced molybdenum oxide nanocrystals.

Selective Thermal Reduction of Single-layer MoO_3…, Deng, etal. SUSC-D—06-00862

3

In this work, we demonstrate that it is possible to achieve selective reduction of these ordered MoO_3 monolayer nanocrystals on Au(111).In principle, Mo has three stable oxidation states: Mo^{6+}, Mo^{5+} and Mo^{4+}. Recently, the group of Hrbek reported on the reduction of ramified MoO_3 nanoclusters on the Au(111) surface prepared by NO_2-induced oxidation of Mo nanoclusters at 500 K [15, 16]. The reduction of these MoO_3 nanoclusters during annealing to 700 K was accompanied by a loss of Mo species, and resulted in a mixture of Mo^{+5} and Mo^{+6} species [15, 16]. STM showed that the reduced MoO_x structures remained 2-dimensional, but did not provide insight into the distribution of the reduced Mo atoms, in part because of structural disorder. Lower oxidation states of Mo such as Mo^{+4} can be prepared by oxidation of Mo metal by O_2 exposure. In this case, the full oxidation to Mo^{+6} seems to be kinetically hindered.

Herein, we report on both theoretical and experimental studies on the thermal reduction of two-dimensional MoO_3 nanocrystallites. Crystalline nanoparticles are more amenable to study using theory and experiment. As described in a previous publication, the synthesis of fully oxidized and well-ordered MoO_3 nanostructures on Au(111) requires iterative Mo deposition and oxidation with NO_2 [13]. Similar to bulk MoO_3, the reduction of these single-layer MoO_3 nanocrystals seems to proceed via shear defect formation which results from one-dimensional ordering and elimination of oxygen vacancies. The oxidation state of Mo associated with these shear-plane defects is +5. The percentage of Mo in the +5 state increases as a function of annealing time, up to a maximum of 50% at 650 K. This provides us with a methode to tailor the growth of reduced molybdenum oxide nanostructures with controllable oxidation states.

Methods

Selective Thermal Reduction of Single-layer MoO_3…, Deng, etal. SUSC-D—06-00862

Experimental

The experiments were performed in three separate ultrahigh vacuum (UHV) systems, all described previously. Scanning tunneling microscopy experiments were performed in a commercial ultrahigh vacuum system with a base pressure of 5×10^{-11} mbar. The system has separate compartments for sample preparation, e.g., Mo evaporation, and sample characterization. The characterization compartment is equipped with commercial instrumentation for scanning probe microscopy (Omicron), Auger electron spectroscopy (AES), and low energy electron diffraction (LEED).

The XPS chamber (base pressures $\sim 8 \times 10^{-10}$ mbar) is equipped with a low-energy electron diffraction (LEED) equipment, a quadrupole mass spectrometer (UTI 100C) for temperature programmed reaction experiments and an XPS system (PHI ESCA 5300) consisting of an X-ray source and a hemispherical analyzer.

The HREELS chamber (base pressure $\sim 5 \times 10^{-10}$ mbar) is equipped with a commercial high-resolution electron energy loss spectrometer (LK technologies, model LK-2000-14-R), a LEED equipment, a quadrupole mass spectrometer (UTI 100C) and an Auger electron spectrometer (Perkin-Elmer model 15-555).

In all systems, the clean Au(111) surface was prepared by cycles of Ar^+ sputtering (1000 eV) at 300 K, followed by annealing at 900 K for 5 minutes and 700 K for 1 hour. This procedure was repeated until no impurities, e.g. carbon, oxygen, or Mo, were detected using either XPS or Auger electron spectroscopy. The presence of the 'herringbone' reconstruction, inherent to clean Au(111) surfaces, was verified by the presence of satellite spots in the Au(111) LEED patterns.

MoO_3 nanostructures were prepared by oxidation of Mo nanoclusters using NO_2. Deposition

Selective Thermal Reduction of Single-layer MoO_3…, Deng, etal. SUSC-D—06-00862

5

of Mo nanoclusers could be achieved either by chemical vapor deposition (CVD) or by physical vapor deposition (PVD). In the CVD method, $Mo(CO)_6$ (98 %) and NO_2 (Matheson, 99.5%) were dosed iteratively [13]: the reconstructed Au(111) surface was alternatively exposed to 1 L $Mo(CO)_6$ and 10 L NO_2 at 450 K. After four iterations, the sample was heated (dT/dt ≈ 5 K/second) and maintained at 600 K for 1 minute. This cycle was repeated four times such that the total exposure to $Mo(CO)_6$ and NO_2 was 16 L and 160 L, respectively. In the PVD method, molybdenum (Goodfellow, 99.9%) was evaporated from rod material (~1.5 mm diameter) using an electron beam evaporator (Omicron) (900 V/~65 mA) followed by exposure to NO_2 (Matheson, 99.5%) at 500 K with a typical pressure of 1×10^{-7} Torr, as described in detail elsewhere [14]. In the present studies, we used the CVD method to prepare MoO_3 nanostructures in XPS and HREELS chambers and the PVD method in the STM system. Importantly, both methods yield identical MoO_3 nanostructures, as confirmed by STM and LEED in earlier studies [13], [14].

All XPS spectra were collected at room temperature with a pass energy of 22.36 eV using Mg Kα radiation (($h\nu$ = 1253.6 eV). The binding energy was calibrated by Au $4f_{7/2}$ = 84.0 eV for each spectrum. All HREELS (vibrational) spectra were collected at room temperature with a beam energy of 6.91 eV. The typical full width at half-maximum (FWHM) is ~70 cm^{-1}. STM images were collected at room temperature. Z-channel (topography) and I-channel (constant height) images were obtained simultaneously. Etched $Pt_{0.8}Ir_{0.2}$ tips from molecular imaging were used for imaging.

The XPS data analysis involved satellite and non-linear background subtraction, curve-fitting (mix Gaussion-Lorentzian function with 85% of Gaussion) and peak area determination by integration of both Mo $3d_{3/2}$ and $3d_{5/2}$ peaks. The Mo 3d region was fitted by doublets with

Selective Thermal Reduction of Single-layer MoO$_3$…, Deng, etal. SUSC-D—06-00862

fixed spectroscopic parameters, such as spin-orbit separation (3.1 eV), $Mo(3d_{3/2})$-$(3d_{5/2})$ intensity ratio (R = 0.66) and full width at half maximum (FWHM = 1.7 eV), but with independent and variable positions and intensities as optimized by the program.

Theoretical

Density functional theory (DFT) calculations employed the projected augmented wave method [Kresse, 1999 #4010;Blochl, 1994 #4011] and the Perdew-Wang 91 gradient correction for the exchange-correlation functional, as implemented in VASP [17]. We model the Au(111) surface by a slab of 6 Au layers, separated by 16.5 Å of vacuum before the oxide is introduced, and the oxide and top 3 Au layers were relaxed. Further computational details can be found in our previous publication [1].

Results and discussion

As-prepared MoO₃ nanostructures

As described above, ordered two-dimensional MoO_3 nanostructures on Au(111) can be produced via oxidation of Mo nanoclusters by NO_2 exposure. The required Mo nanoclusters can be prepared by chemical vapor deposition (CVD) using molybdenum hexacarbonyl as a Mo precursor or by physical vapor deposition (PVD). Both techniques result in the growth of well-ordered, 2D MoO_3 islands as confirmed by STM and LEED [13][14]. For example, the characteristic $c(4 \times 2)$ LEED pattern displayed in Figure 1 was obtained from MoO_3 nanostructures on Au(111) prepared by the CVD method in the XPS chamber. The pattern is identical to those observed in our earlier STM studies [13], indicating that the same structure was prepared.

Selective Thermal Reduction of Single-layer MoO₃…, Deng, etal. SUSC-D—06-00862

7

XPS results demonstrate that the Mo in these oxide structures is essentially fully oxidized—in the +6 state—except for a small percentage of defects (Figure 2). Specifically, the predominant oxidation state is signified by the peaks with binding energies of 232.3 eV (Mo $3d_{5/2}$) and 235.4 eV (Mo $3d_{3/2}$) which are similar to the binding energies reported for bulk MoO_3 (BE = 232.3-232.8 eV; thus indicating the formation of MoO_3. A weak shoulder at lower binding energy indicates the possible presence of a small percentage of Mo^{5+}. Based on the signal intensities of the Mo $^{+5}$ related peaks at 231. 1 and 234.2 eV, as much as 6% Mo^{5+} may be present.

The ability to nearly fully oxidize Mo so as to form ordered monolayer nanocrystals provides a starting point to control the oxidation states of these oxides. Iterative dosing of $Mo(CO)_6$ and NO_2 was necessary due to the kinetic control of oxidation: full oxidation of Mo is most readily effected with initially small Mo clusters (< 5nm) as starting material [13], whilst partially oxidized Mo with lower oxidation states, such as Mo^{5+} and Mo^{4+} , was observed when Mo clusters were larger. Growth of larger MoO_3 islands can be achieved by iterative deposition /oxidation cycles. For example, after 16 cycles well-ordered islands were found to be 600 nm^2 on average, yielding a clear $c(4\times2)$ LEED pattern. No LEED pattern of MoO_3 on Au(111) was reported by Z. Song et al.[16], possibly due to the ramified oxide structure, or smaller island size.

As mentioned above, a small fraction of Mo^{5+} was observed in the MoO_3 nanostructures . Importantly, this small amount of Mo^{5+} persisted even after extensive dosing of NO_2. In our study, 20 L NO_2 was used instead of 10 L NO_2 for each iterative dosing, and the resultant XP spectrum still yields about 6% Mo^{5+}. This result indicates the presence of a small percentage of defects in the structure, which has been observed in STM studies as well [14].

Selective Thermal Reduction of Single-layer MoO_3…, Deng, etal. SUSC-D—06-00862

8

We have previously proposed a model for the atomic structure of a continuous 2D layer of single-layer MoO_3 on Au(111). The model is consistent with LEED, STM (CVD and PVD), XPS (oxidation state: Mo^{6+}) and HREELS results [1].

Thermal reduction of MoO$_3$ nanostructures at 650 K

The Mo^{5+} related XPS signal increases in intensity upon annealing to 650 K (Figure 3a). Specifically, annealing to 650 K for 20 minutes results in a broadening of Mo 3d peaks, which can be fitted a mixture of 70% Mo^{6+} and 30% Mo^{5+} with binding energies of 232.5 eV and 231.4 eV for Mo $3d_{5/2}$, respectively. The fraction of Mo in the +5 oxidation state further increases with increasing annealing time, and ultimately a 1:1 mixture of Mo^{5+}:Mo^{6+} is formed after annealing at 650 K for 1 hour (Figure 3a). No further changes in the Mo^{5+}:Mo^{6+} ratio were observed upon heating for longer times, up to 120 minutes (Figure 3b). Furthermore, no other oxidation states were detected after heating to 650 K in any of our experiments. Specifically, no Mo^{4+} is formed, based on the absence of intensity in the Mo $3d_{5/2}$ region at 229.1 eV.

The partial reduction of Mo^{+6} to Mo^{+5} is accompanied by the loss of a small amount of Mo based on the integrated intensities of Mo 3d region (Figure 3b). Specifically, the total amount of Mo decrease by ~ 6%/8%/10% during annealing at 650 K for 20/40/60 minutes. Finally, 88% Mo remains on the Au surface upon annealing at 650 K for 120 minutes. The small loss of Mo is probably the result of some dissolution of Mo into the bulk associated with reduction or desorption of MoO_3 molecules during annealing.

The partial reduction of Mo^{+6} during annealing also causes changes in the vibrational spectra (Figure 4). Before annealing, the most intense peak is found at 850 cm^{-1} with a shoulder at 990 cm^{-1} (Figure 4(i)), and two less intense peaks are observed at 480 and 280 cm^{-1}. Based on

Selective Thermal Reduction of Single-layer MoO$_3$…, Deng, etal. SUSC-D—06-00862

9

DFT calculations on the MoO_3 structure, the peaks at 990 cm^{-1} and 850 cm^{-1} can be assigned to stretches of the terminal O and bridging O bonds respectively, whilst the other modes involve the bending of bridging O bonds, and to a lesser extent, terminal O bonds. The atomic structure of the ordered MoO_3 monolayer phase on Au(111) including the positions of terminal and bridging oxygen atoms is shown in Figure 5(a). Annealing the MoO_3 nanostructures to 650K results in a decrease of the peak intensities (Figure 4(ii)-(iv)). Specifically, the peak intensity of the 850 cm^{-1} bridging O stretch deceases to about 80% after 20 minutes of annealing, and to about 20% after 60 minutes. The lower frequency peaks also decrease. Meanwhile, the terminal oxygen stretch peak resolves upon annealing. Although a decrease in peak intensity is also observed for the terminal O stretch, the ratio of peak intensities for the bridging and terminal O stretches changes from 4:1 to 2:1, indicating a structural change. The fact that the terminal oxygen related vibrational modes are less affected by the reduction process is a first indication that the reduced Mo oxide remains a two-dimensional structure

Proposed model for thermally reduced oxide

We propose that reduction of the MoO_3 monolayer structures involves the formation of shear defects similar to of the shear planes found in the so-called Magneli phases of reduced bulk Mo-trioxide, Mo_nO_{3n-1} [18]. Such shear defects could eliminate one-dimensionally ordered arrays of oxygen vacancies formed during annealing by a local transformation (shearing) from corner-connected to edge-connected MoO_3 units. [lit20] In the case of the Magneli phases of reduced bulk Mo-trioxide, the shear planes are regularly spaced indicating a mutual elastic repulsion.. The driving force for shear plane formation seems to be the stabilization of isolated oxygen

Selective Thermal Reduction of Single-layer MoO_3…, Deng, etal. SUSC-D—06-00862

vacancies by migration towards one another to form shear planes of edge-sharing MoO_6 octahedra. The shear planes can then expand by trapping more vacancies [18].

Similarly, the reduction of 2D MoO_3 islands could cause the formation of one-dimensional shear defects which would lead to the elimination of the oxygen vacancies formed during thermal reduction. The formation of these shear defects involves a local transformation of corner-connected MoO_4 tetrahedra to edge-connected MoO_4 tetrahedra (Figures 5b and 6e). This scenario seems to be supported by STM. Figure 6 shows STM images collected from MoO_3-covered Au(111) surfaces before (a) and after annealing at T > 650K (b-d). The stoichiometric MoO_3 islands shown in Figure 6a were prepared by PVD of Mo (~0.2 ML) and subsequent oxidation with NO_2 at 500 K. These MoO_3 islands exhibit an apparent height of ~0.5 nm [14]. Annealing at T > 650 K leads to several changes: (i) the MoO_3 islands grow considerably in size (Figure 6b); (ii) extended, one-dimensional defects appear on top of the MoO_{3-x} islands (Figure 6c) which (iii) separate regions shifted by half a lattice constant (Figure 6d), and (iv) the Mo coverage decreases by ~ 60% (suggesting that the actual annealing temperature was slightly higher than 650 K). Clearly, the reduced Mo oxide has a two-dimensional structure despite the large scale mass transport required for the observed morphological changes. The Z-channel STM image shown in Figure 6c reveals that the surface corrugation on top of the reduced MoO_3 island is less than 0.1 nm. A possible structural model of a reduced single-layer MoO_3 island is shown in Figure 6e. The model assumes the formation of shear planes by a local transformation of corner connected MoO_3 units to edge connected MoO_3 units, and is capable of reproducing the main features observed in the high resolution STM image shown in Figure 6d. Specifically, it predicts the observed shift of the MoO_3 lattice by half a lattice constant between regions separated by a shear defect. The average spacing between the line defects shown in Figure 6c,d is

Selective Thermal Reduction of Single-layer MoO_3…, Deng, etal. SUSC-D—06-00862

11

approximately 1.5 nm which according to the shear model shown in Figure 6e would correspond to Mo^{+5} fraction of 40%.

Figure 7 shows a relaxed shear defect structure in which one bridging O is lost for every four Mo. The defect is characterized by more closely-spaced Mo rows connected by 3-fold coordinated O (3-fold coordinated O is also present in bulk MoO_3). The bond lengths of $Mo-O_a$ and $Mo-O_b$ in the defect structure are, respectively, in the range (-5.1, +5.1)% and (-4.6, +6.2)% of their corresponding values in the fully oxidized oxide. The bond length of $Mo-O_t$ remains unchanged consistent with the vibrational spectra shown in Figure 4. The longest Mo-O bonds (2.08 Å) are those joining Mo^{5+} to a 3-fold coordinated O atom across the defect line. The formal oxidation state of Mo is +6 and +5 between and along the shear defects respectively, and no Mo^{4+} is present. This structure is consistent with X-ray photoelectron data. The loss of bridging O in the shear structure is also consistent with vibrational peak intensities, which indicate a sharper drop in the intensity for the bridging O stretch compared to that for the terminal O stretch. The formation of shear defects is further corroborated by the observation that the lattice planes on both sides of these defects are shifted by half a lattice constant with respect to each other (Figure 6). Finally, the 1D defects imaged in STM (Figure 6) are in approximately the same orientation as predicted by our model; that is in the experimental STM image, these defects are at an angle of about 42° relative to the <1-10> direction of Au. Simulating STM images in the Tersoff-Hamann approximation results in a bright line representing the shear plane defect, which makes an angle of 41° relative to the <1-10> direction, in agreement with experiment (Figure 7c).

From the projected density of states of the theoretical model (Figure 8), it can be seen that Mo atoms associated with the shear defect have a higher density of states at the Fermi level than those away from the defect or those in the fully-oxidized oxide, suggesting possible enhanced

Selective Thermal Reduction of Single-layer MoO_3…, Deng, etal. SUSC-D—06-00862

reactivity (especially involving loss of O) along shear planes. The predominant contribution to Fermi level states arises from d states of Mo^{5+} (Figure 8a). The density of states of O bridging atoms in the shear plane region, both of O_a and O_b type, are significantly shifted compared to those of corresponding sites far from the defect. This is the result of an increase in coordination number of these O atoms (2 away from the defect and 3 in the defect region), and changes in the oxidation state of Mo atoms in the defect region, to which these O bridging atoms are bonded.

The shear defects may exhibit different reactivity and interesting electrical properties due to the presence of the oxygen vacancies. The ability to quantitatively control defects and oxidation states is the key toward demonstrating the effect of defects and specific oxidation states on oxidation reactions. Our results above clearly show that single-layer MoO_3 nanostructures on Au(111) can be selectively reduced in a controllable manner that depends on annealing temperature and duration. In addition, the resulting molybdenum oxide structures may also present exciting possibilities for other applications, e.g. chemical sensors.

Limitations of model and other possible structures

It is important to note that the theoretical model proposed here may not accurately represent the experimental system, because the model assumes an infinitely long defect structure. This difference may account for discrepancies between the STM simulation and experimental image, such as the shorter length of defects and presence of black spots in the experimental image, which also contains a smaller density of defects. Systems involving finite-length-defects or lower densities of defects are more complex and computationally demanding. However, the model represents a possible local atomic structure at the defects and is consistent with experimental results.

Selective Thermal Reduction of Single-layer MoO_3…, Deng, etal. SUSC-D—06-00862

The final composition of 1:1 for the ratio of Mo^{5+} to Mo^{6+}, obtained with prolonged

annealing, corresponds to the well-defined stoichiometry Mo_4O_{11}. It is interesting that bulk

Mo_4O_{11} is the Magneli phase with the highest known density of shear defects [18]. Bulk Mo_4O_{11}

has a three-dimensional (3D) structure, with layers of Mo_6O_{22} linked by MoO_4 tetrahedra *via*

covalent bonds [Canadell, 1989 #4012]. It is possible that the final stable Mo_4O_{11} phase observed

in our experiments is the two-dimensional analog to the three-dimensional Mo_4O_{11} bulk phase.

This would present exciting opportunities for fundamental studies because bulk Mo_4O_{11} exhibits

charge density wave transitions [Canadell, 1989 #4012], and it would be interesting to determine

how a metallic substrate would affect this phenomenon. The fact that we do not observe the

formation of a three-dimensional Mo_4O_{11}phase indicates the presence of kinetic barriers. Indeed,

a 3D Mo oxide phase can be grown on Au(111) if the Mo deposition is performed in an ambient

of NO_2 at 500 K (unpublished results)..Further STM studies will be necessary to refine the

structural model described in this work.

Conclusions

Well-ordered Mo oxide nanostructures on Au(111) have been prepared via deposition of

metallic Mo (CVD or PVD) followed by oxidation using NO_2 as a reactant. The observation of a

well-ordered *c*(4×2) LEED pattern proves the formation of a crystalline epitaxial Mo oxide. XPS

indicates that this oxide is MoO_3, with up to 6% of Mo^{5+} defects. Upon annealing at 650 K, these

MoO_3 nanostructures are selectively reduced to Mo^{5+} indicating the formation of oxygen

vacancies. The percentage of Mo^{5+} and the corresponding oxygen vacancies increases with

increasing annealing time until the stable composition Mo_4O_{11} (50% Mo^{+5}) is reached after one

hour at 650 K. Further reduction towards Mo^{4+} has not been observed. This simple annealing

Selective Thermal Reduction of Single-layer MoO_3…, Deng, etal. SUSC-D—06-00862

14

treatment allows one to fine-tune the concentration of Mo^{5+} in the resulting selectively reduced structures by controlling the temperature and annealing time.

Based on our preliminary STM results, the thermal reduction of MoO_3 nanostructures on Au seems to lead to the formation of shear defects, similar to those observed in reduced bulk MoO_3. .The driving force for the formation of these shear defects could be the elimination of oxygen vacancies produced by annealing. However, in contrast to the 3D structures observed in reduced bulk MoO_3, the reduced MoO_3 islands on Au(111) remain pure 2D structures..The formation of 3D structures in our model system has only been observed if Mo deposition is performed in an ambient of NO_2 Thus the reduced 2D Mo oxide structures described in this paper are distinctly different from the 3D structures found in reduced bulk MoO_3, and therefore provide an interesting platform for further studies. The ability to control and tailor the oxidation states in these novel oxide structures on metal surfaces suggests exciting possibilities for future applications. Further STM studies of the final Mo_4O_{11} structure will be necessary to refine the structural model.

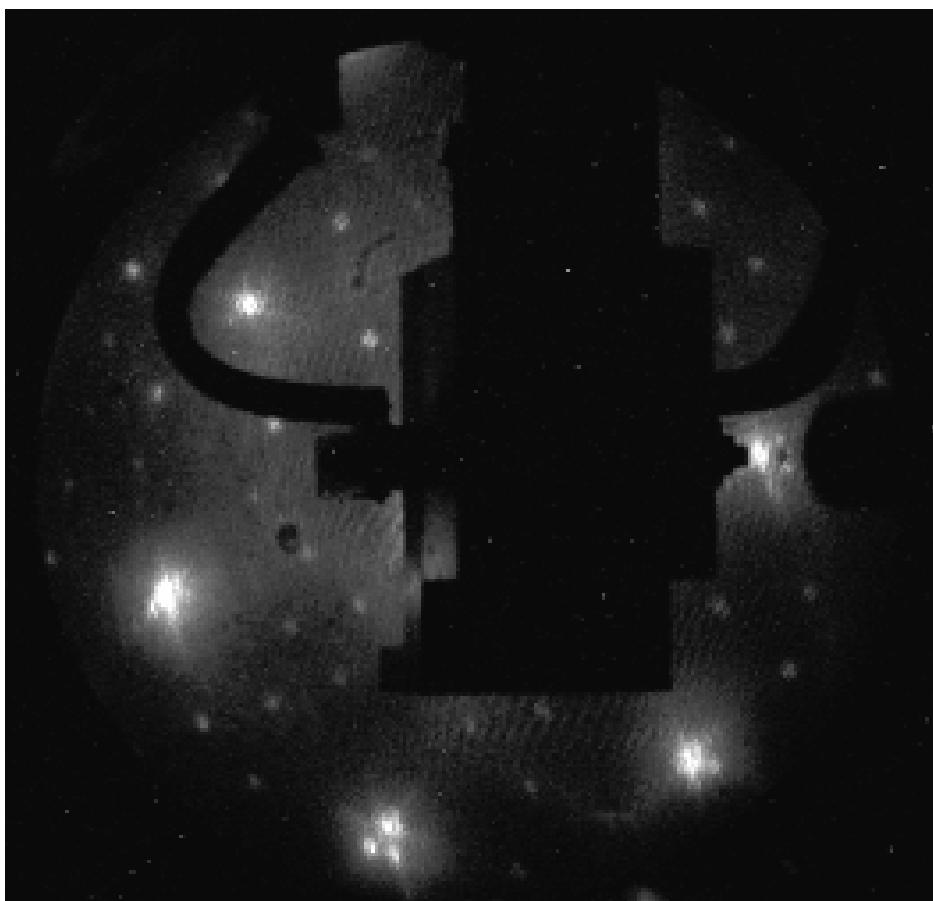Selective Thermal Reduction of Single-layer MoO_3…, Deng, etal. SUSC-D—06-00862

15

Selective Thermal Reduction of Single-layer MoO$_3$…, Deng, etal. SUSC-D—06-00862

16

Figure Captions

Figure 1. LEED patterns obtained at 300 K showing a c(4×2) structure after iterative dosing. The beam energy was 77 eV. This pattern is identical to that previously reported [13], [14].

Selective Thermal Reduction of Single-layer MoO$_3$…, Deng, etal. SUSC-D—06-00862

17
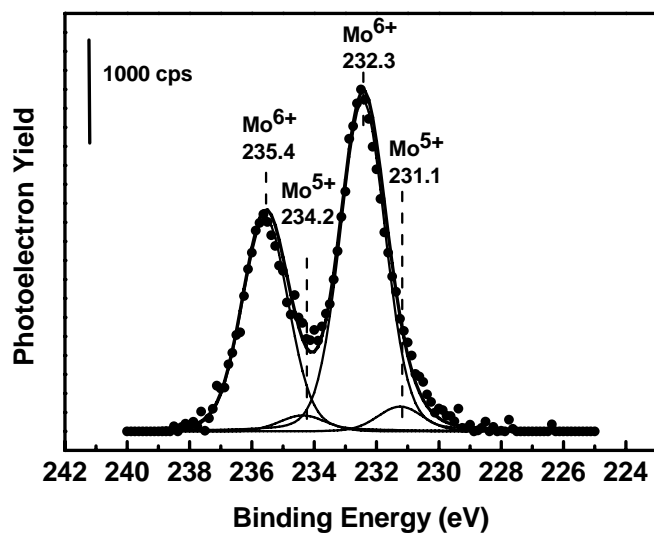
Figure 2. X-ray photoelectron spectrum for the Mo 3d region obtained after preparation of the oxidized Mo nanocrystals on Au(111) using iterative dosing of $Mo(CO)_6$ and NO_2. The total spectrum was fitted by ~94% Mo^{6+} ($3d_{5/2}$, 232.3 eV) and ~6% Mo^{5+} ($3d_{5/2}$, 231.1 eV). The curve fitting parameters and methods were described in detail in the experimental section.

Selective Thermal Reduction of Single-layer MoO_3…, Deng, etal. SUSC-D—06-00862

18
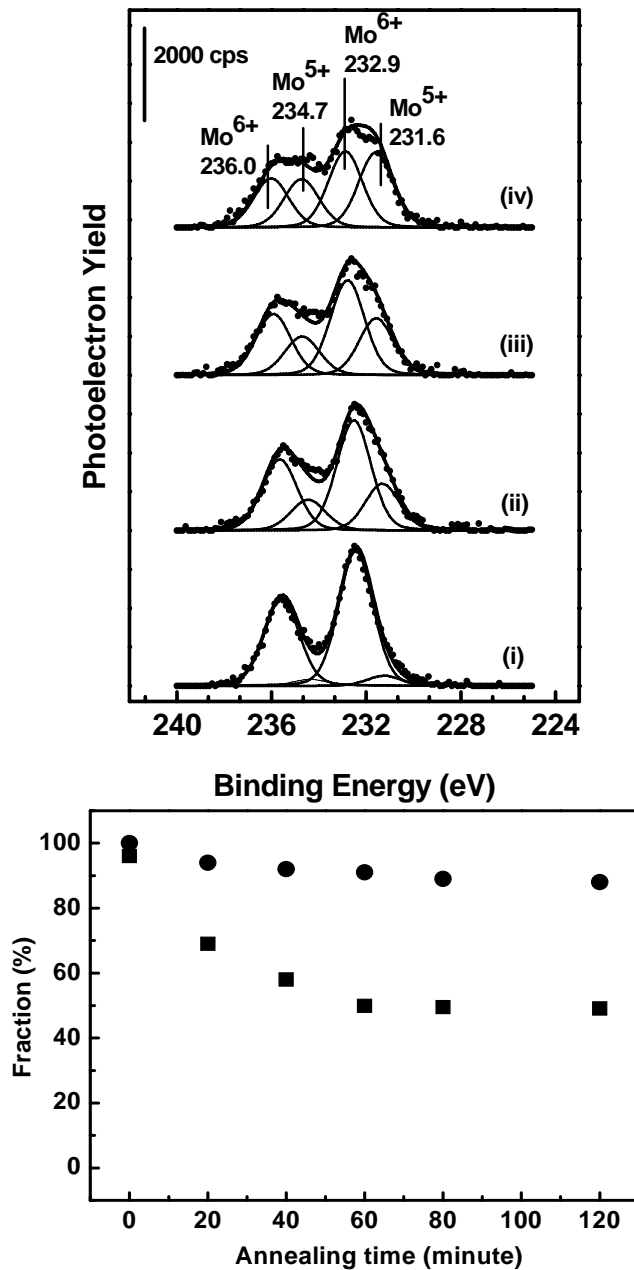
Figure 3. X-ray photoelectron data for the Mo 3d region showing the reduction of MoO_3 nanostructures on Au(111) prepared by iterative dosing of $Mo(CO)_6$ and NO_2. (a) Spectra for: (i) as-prepared material; and followed by annealing to 650 K for (ii) 20 min; (iii) 40 min; (iv) 60 min. All spectra were obtained at room temperature. (b) Corresponding data showing the fraction of Mo in the 6^+ oxidation state (square) and the fraction of Mo remaining on the surface (circle) referenced to the as-prepared sample.

Selective Thermal Reduction of Single-layer MoO_3..., Deng, etal. SUSC-D—06-00862

19
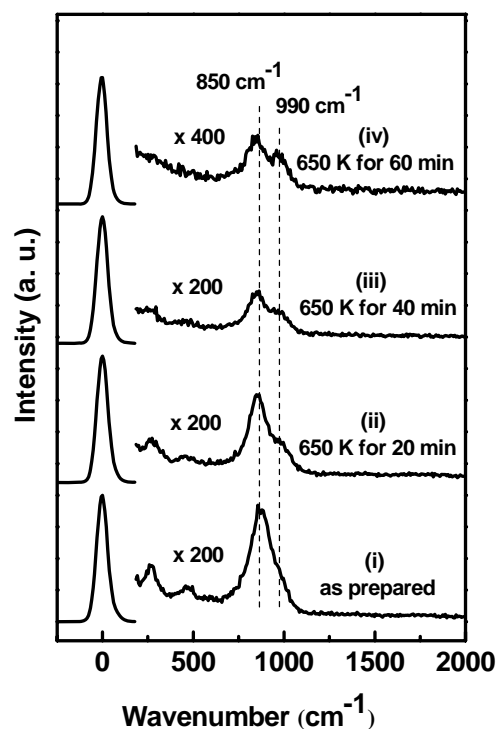
Figure 4. Vibrational (HREEL) spectra obtained after preparing MoO_3 nanostructures on Au(111) by 16 iterations of dosing. The spectrum (i) is taken after the formation of MoO_3 without further annealing. The top three spectra are obtained after annealing to 650 K for (ii) 20 minute, (iii) 40 minute and (iv) 60 minute. The FWHM is typically ~70 cm^{-1}. All spectra were collected at room temperature.

Selective Thermal Reduction of Single-layer MoO_3…, Deng, etal. SUSC-D—06-00862

20
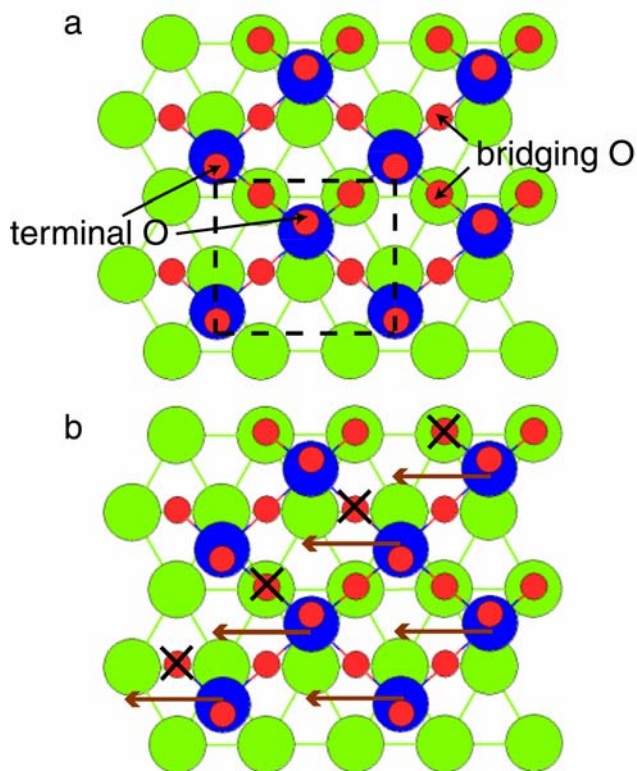
Figure 5. (a) Atomic structure of MoO_3 monolayer on Au(111). (b) Schematic showing the formation of shear defects. The dotted black box in (a) denotes the $c(4\times2)$ unit cell. The structure is repeated periodically in the plane of the Au surface. Only the top Au layer is shown (out of a total of 6 layers), as indicated by the hexagonal lattice of green circles. The [1-10] direction of Au is indicated. Mo and O are represented respectively by large blue and small red circles. Terminal (O_t) and bridging O's (O_a and O_b) are labeled in (a). The subscripts for O_a and O_b indicate if the bridging O is on an atop or bridging site of the Au(111) surface. The schematic in (b) shows how the oxide structure can 'shear' in the direction of the arrow, to accommodate the loss of a row of bridging O's as marked by black crosses.

Selective Thermal Reduction of Single-layer MoO_3…, Deng, etal. SUSC-D—06-00862

21
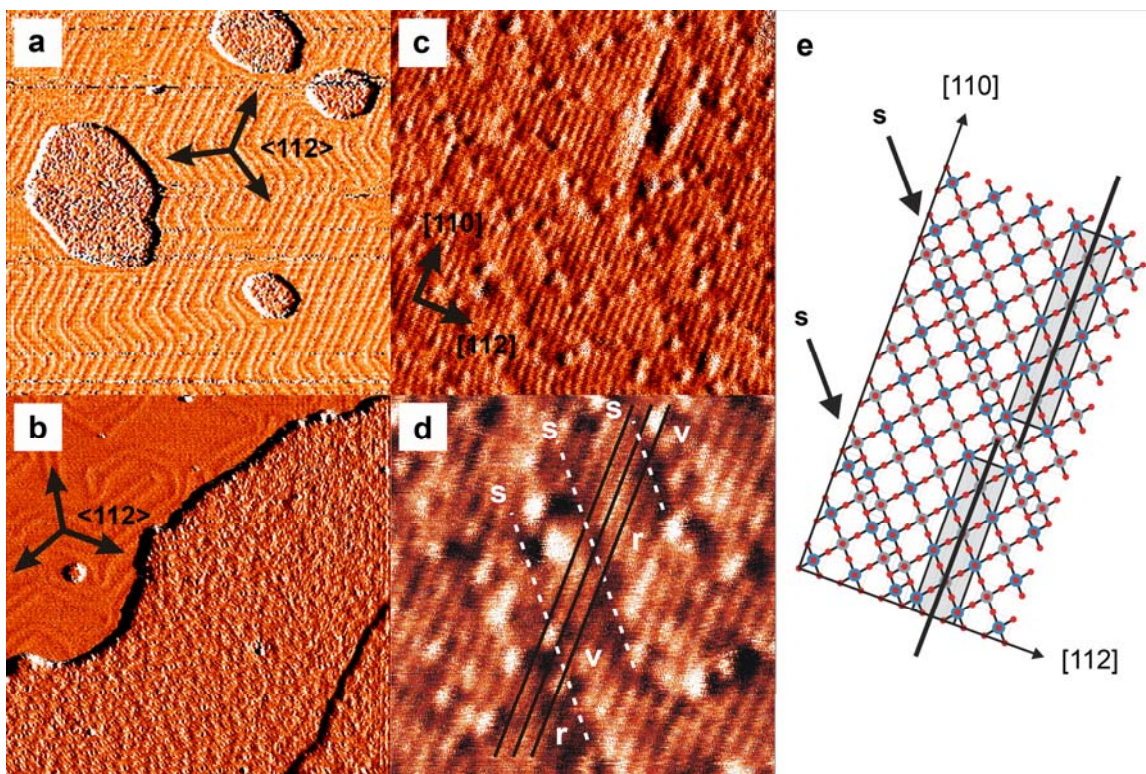
Figure 6. STM images collected from MoO_3-covered Au(111) surfaces before (a) and after annealing at T > 650K (b-d): (a) Stoichiometric MoO_3 islands on Au(111) prepared by PVD of Mo and subsequent oxidation with NO_2 at 500 K. The apparent island height is ~0.5 nm (*I*-channel, 125 nm x 125 nm). (b) Reduced Mo oxide island formed after annealing at T > 650 K (*I*- channel, 85 nm x 85 nm). Note the increase in size of the Mo oxide island. (c) Higher magnification STM image of the reduced Mo oxide island shown in (b). Despite the appearance of defects, the surface corrugation on top of the island is less than 0.1 nm demonstrating the 2D character of the structure (*Z*- channel, 17 nm x 17 nm, vertical color scale is 0-0.125 nm). (d) Extended, one-dimensional defects marked by dashed lines (*s*) appear on top of the Mo oxide islands and separate regions shifted by half a lattice constant. The full lines serve as a visual guide to demonstrate the lattice shift from a valley (*v*) to a ridge (*r*) position on opposite sites of the defect (*s*) (*I*- channel, 8 nm x 8 nm. (e) Structural model of a reduced single-layer MoO_3 island. Note that the presence of shear planes causes a shift of the MoO_3 lattice by half a lattice constant between regions separated by a shear defect.

Selective Thermal Reduction of Single-layer MoO_3…, Deng, etal. SUSC-D—06-00862

22
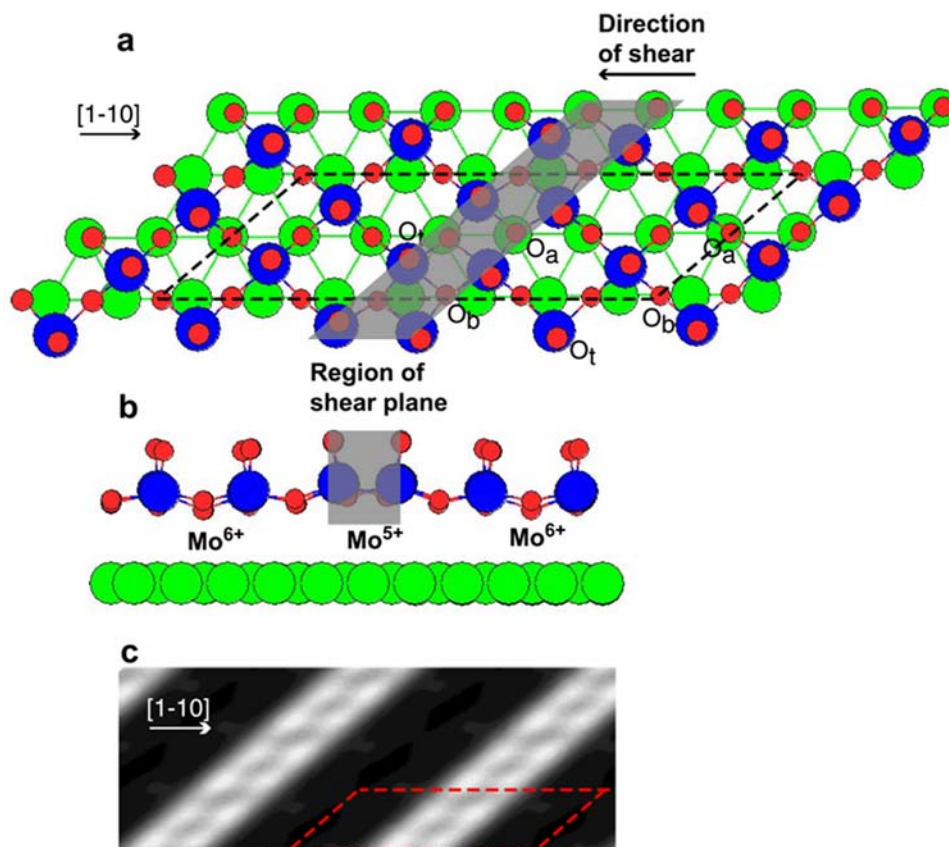
Figure 7. Relaxed shear defect structure, (a) top view and (b) side view. (c) STM simulation with a sample bias of 1.5 V, with Gaussian smearing (standard deviation of 1.2 Å) to take into account tip convolution effects. The unit cell used in this model is indicated by a dashed black box in (a) and a dashed red box in (c). The defect region is shaded in gray in (a) and (b). The bright area in the STM simulation (c) corresponds to the shear plane defect. Mo atoms in the defect are raised by ~ 0.3 Å relative to those away from the defect, which are in turn ~ 3.7 Å above the top Au layer (6 % more than corresponding height in the perfect oxide (Figure 5)).

Selective Thermal Reduction of Single-layer MoO_3…, Deng, etal. SUSC-D—06-00862

23
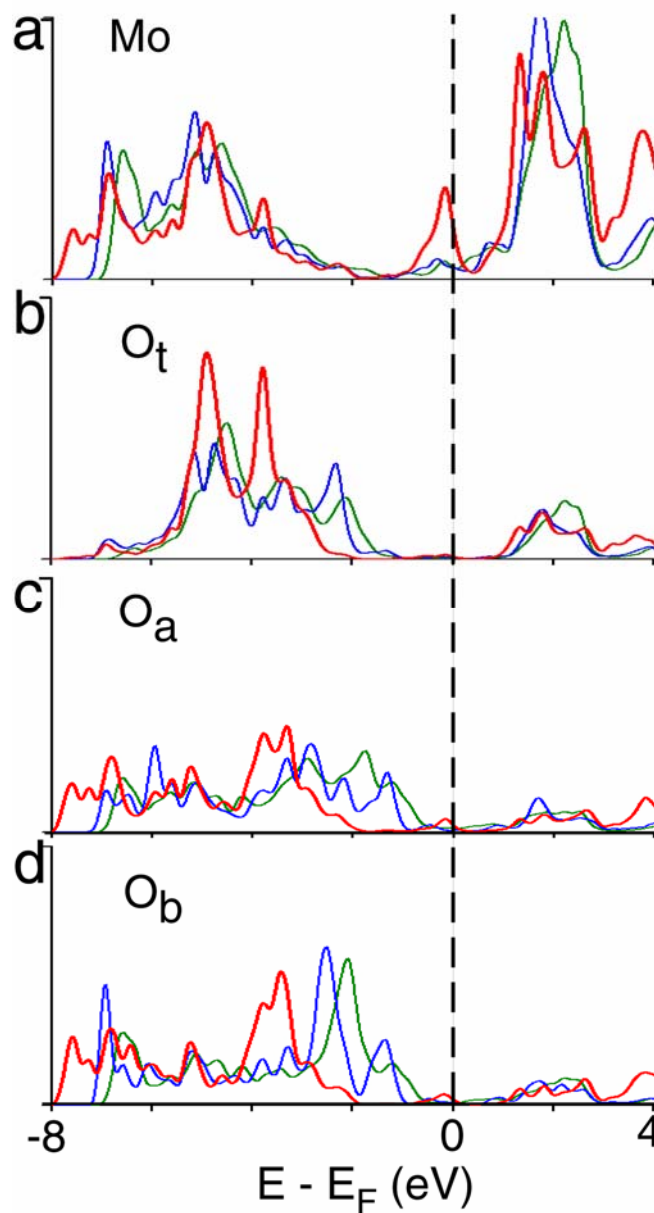
Figure 8. Electronic densities of states projected onto (a) Mo, (b) O_t, (c) O_a and (d) O_b, summed over s, p and d contributions. Red (thickest), blue and green (finest) curves respectively represent atoms at the shear defect, atoms mid-way between the defects in the reduced oxide (Figure 7), and atoms in the fully oxidized oxide (Figure 5).

Selective Thermal Reduction of Single-layer MoO_3…, Deng, etal. SUSC-D—06-00862

References

1. Quek, S.Y., M.M. Biener, J. Biener, C.M. Friend, and E. Kaxiras, *Tuning electronic properties of novel metal oxide nanocrystals using interface interactions: MoO₃ monolayers on Au(111).* Surface Science Letters, 2005. **577**: p. L71-L77.
2. Henrich, V.E. and P.A. Cox, *The Surface Science of Metal Oxides.* 1994, Cambridge: Cambridge University Press.
3. Spencer, P.J., *Process and Catalyst for the Production of Formaldehyde from Methane.* United States Patent, 1986. **4,607,127**(August 19).
4. Spencer, N.D. and C.J. Pereira, *Partial oxidation of CH₄ to HCHO over a MoO₃-SiO₂ catalyst: A kinetic study.* AIChE Journal, 1987. **33**(11): p. 1808-1812.
5. Spencer, N.D., *Partial Oxidation of Methane to Formaldehyde by Means of Molecular Oxygen.* Journal of Catalysis, 1988. **109**: p. 187-197.
6. Banares, M.A., N.D. Spencer, M.D. Jones, and I.E. Wachs, *Effect of Alkali Metal Cations on the Structure of Mo(VI)/SiO₂ Catalysts and Its Relevance to the Selective Oxidation of Methane and Methanol.* J.Catal., 1994. **146**: p. 204-210.
7. SalehAlhamed, Y.A., R.R. Hudgins, and P.L. Silveston, *Role of water vapor in the partial oxidation of propene.* Journal of Catalysis, 1996. **161**(1): p. 430-440.
8. Deiner, L.J., A.S.Y. Chan, M.A. Sheehy, and C.M. Friend, *The Reaction of CH₃NO₂ on O-covered Mo(110): The Effect of Oxygen on Product Distribution.* Surface Science Letters, 2004. **555**(1-3): p. L127-L132.
9. Surnev, S., G. Kresse, M.G. Ramsey, and F.P. Netzer, *Novel interface-mediated metastable oxide phases: Vanadium oxides on Pd(111).* Physical Review Letters, 2001. **8708**(8).
10. Costello, C.K., J. Guzman, J.H. Yang, Y.M. Wang, M.C. Kung, B.C. Gates, and H.H. Kung, *Activation of Au/gamma-Al2O3 catalysts for CO oxidation: Characterization by X-ray absorption near edge structure and temperature programmed reduction.* Journal of Physical Chemistry B, 2004. **108**(33): p. 12529-12536.
11. Liu, Z.P., C.M. Wang, and K.N. Fan, *Single gold atoms in heterogeneous catalysis: Selective 1,3-butadiene hydrogenation over Au/ZrO2.* Angewandte Chemie-International Edition, 2006. **45**(41): p. 6865-6868.
12. Wang, X.a.W., IE, *Designing the Activity/Selectivity of Surface Acidic, Basic and Redox Active Sites in the Supported K2O-V205/A12O3 Catalytic System.* Catalysis Today, 2004. **96**(4): p. 211-222.
13. Biener, M.M., Friend C.M., *Heteroepitaxial Growth of Novel MoO₃ Nanostructures on Au(111).* Surface Science Letters, 2004. **559**(2-3): p. L173-L179.
14. Biener, M.M., J. Biener, R. Schalek, and C.M. Friend, *Growth of nanocrystalline MoO3 on Au(111) studied by in-situ STM.* J. Chem. Phys., 2004. **121**(23): p. 12010-12016.
15. Chang, Z.P., Z. Song, G. Liu, J.A. Rodriguez, and J. Hrbek, *Synthesis, electronic and chemical properties of MoOx clusters on Au(111).* Surface Science, 2002. **512**(1-2): p. L353-L360.
16. Song, Z., T. Cai, Z. Chang, G. Liu, J.A. Rodriguez, and J. Hrbek, *Molecular Level Study of the Formation and the Spread of MoO3 on Au (111) by STM and XPS.* J. Am. Chem. Soc., 2003. **125**: p. 8059-8066.

Selective Thermal Reduction of Single-layer MoO₃…, Deng, etal. SUSC-D—06-00862

25

17.   Kresse, G. and J. Furthmuller, *Efficient iterative schemes for ab initio total-energy calculations using a plane-wave basis set.* Phys. Rev. B, 1996. **54**(16): p. 11169-11186.

18.   Bursill, L.A., *Crystallographic shear in molybdenum trioxide.* Proc. Roy. Soc. A, 1969. **311**: p. 267-290.

Selective Thermal Reduction of Single-layer MoO_3…, Deng, etal. SUSC-D—06-00862

26